Journal of Materials Chemistry C

Accepted Manuscript

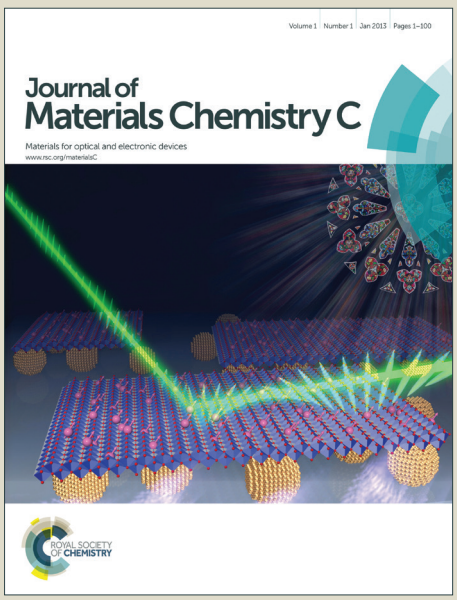

ROYAL SOCIETY OF CHEMISTRY

www.rsc.org/materialsC

Journal Name

RSCPublishing

ARTICLE

Single-Crystalline $La_xNd_{1-x}B_6$ Nanowires: Synthesis, Characterization and Field Emission Performance

Cite this: DOI: 10.1039/x0xx00000x

Qidong Li[a], Hao Zhang[b], Jian Chen[b,*] Yanming Zhao[a,*], Wei Han[a], Qinghua Fan[a], Zhiyong Liang[a], Xudong Liu[a], Quan Kuang[a]

Received 00th January 2012,
Accepted 00th January 2012

DOI: 10.1039/x0xx00000x

www.rsc.org/

We report catalyst-free synthesis of uniform distributed single-crystalline $La_xNd_{1-x}B_6$ nanowires by simply heating mixed La and Nd powders to a proper temperature in an inlet flux of mixed gases (H_2, Ar and BCl_3). FE-SEM, HRTEM, SAED, EDS, element mapping, XRD and Raman scattering results show that $La_xNd_{1-x}B_6$ nanowires are structurally uniform and well-doped single crystal. Based on our experimental results, a dominantly VLS-like mechanism with self-catalytic growth mechanism was proposed and depicted conceptually. The nanowires display excellent field emission performance with low turn-on field of ~4.12V/μm when evaluated as an electron emitter. Attempts were also made to understand the morphological influence of reaction time, reaction temperature and proportion of La and Nd powders.

Introduction

Field emission (FE) is a quantum mechanical process where electrons near the Fermi level can tunnel through an energy barrier and escape to the vacuum level upon application of a high electric field.[1] Recently, substantial research have been carried out on nanostructured materials as field emission cathode materials.[2-6] Since the study and application of rare earth hexaborides ($RE B_6$) as a kind of field emission material, an augment widespread outstanding properties, for instance, the low work function, low volatility at high temperature, high conductivity, high chemical resistance and high mechanical strength, which all manifest their suitability to serve as thermionic electron sources, were revealed by this series of hexaborides.[7] The Fowler-Nordheim (F-N) theory predicts that electron emitters made of materials with a low work function, higher aspect ratio and higher curvature of the tip, could greatly enhance the FE current with a lower applied turn-on voltage.[8] Thus, a lot of relevant research have been carried out on this kind of material with nanostructures attribute especially to the low work function of $RE B_6$. Zhang *et al.* synthesized $R B_6$ (R=La, Gd, Ce) nanowires using $R Cl_3$ and BCl_3 as starting materials through a chemical vapor deposition (CVD) method and excellent field-emission properties were presented by both nanostructured LaB_6 and GdB_6.[9-12] While on account of the severe hygroscopicity of $R Cl_3$ in even low degree of moisture circumstances, it's difficult to obtain large-scale, high quality $R B_6$ nanowires through this method. Brewer *et al.* used $RE Cl_3$ and $B_{10}H_{14}$ as rare earth metal and boron sources respectively together with palladium (Pd) nanoparticles served as catalysts in a similar CVD process.[13-15] Problems are also found in this method. Except for the semblable issue exists in $RE Cl_3$, solid precursor $B_{10}H_{14}$, which is not easy to control in CVD flow, also hinder the synthesis of $RE B_6$. Furthermore, the vacuum and Pd needed in the fabrication process would greatly limit the large-scale production of $RE B_6$ nanowires owing to the cost. Our group developed an effective one-step CVD method based on rare earth metals and BCl_3 gas without any assists of catalysts or templates.[16-17]

As the first commercially used thermionic electron emission source and thermal field-emission material in $RE B_6$ family, LaB_6 present high brightness and long service life.[18] Interest in $RE B_6$ continues to grow, fuelled in part by the successful application. In consequence, NdB_6, which may be the most prominent material with the lowest work function (1.6 eV) in the family of $RE B_6$, is of both great scientific and practical significance to fabricate and seems like to have the potential to replace LaB_6 as next generation FE material. While according to our previous reported literatures,[16-17] it's difficult to synthesize morphologically smooth and geometrically high aspect ratio nanowires both for LaB_6 and NdB_6 using catalyst-free CVD approach, which would greatly influence their behavior as FE materials. As a result, in the present work, we tried to combine La and Nd metal together to synthesize both morphological and geometrical satisfied nanostructured $La_xNd_{1-x}B_6$ for a potential next-generation FE material and explored the possible growth mechanism.

In brief, we have successfully synthesized high-quality, uniform, large-scale $La_xNd_{1-x}B_6$ nanowires via an efficient, one step, easily controlled, catalyst-free CVD method. The morphologies of them turn out to be highly sensitive to the proportion of reactants, reaction temperature and reaction time. $La_xNd_{1-x}B_6$ nanowires are firstly fabricated and reported to the best of our knowledge. Several characterizations affirm their uniform structure and well-doped nature. In addition, the field emission measurement of $La_xNd_{1-x}B_6$ nanowires is also carried out for the first time.

Experimental

All reagents are of analytical grade and used without further purification. Synthesis of $La_xNd_{1-x}B_6$ nanowires was carried out

Journal Name RSCPublishing

ARTICLE

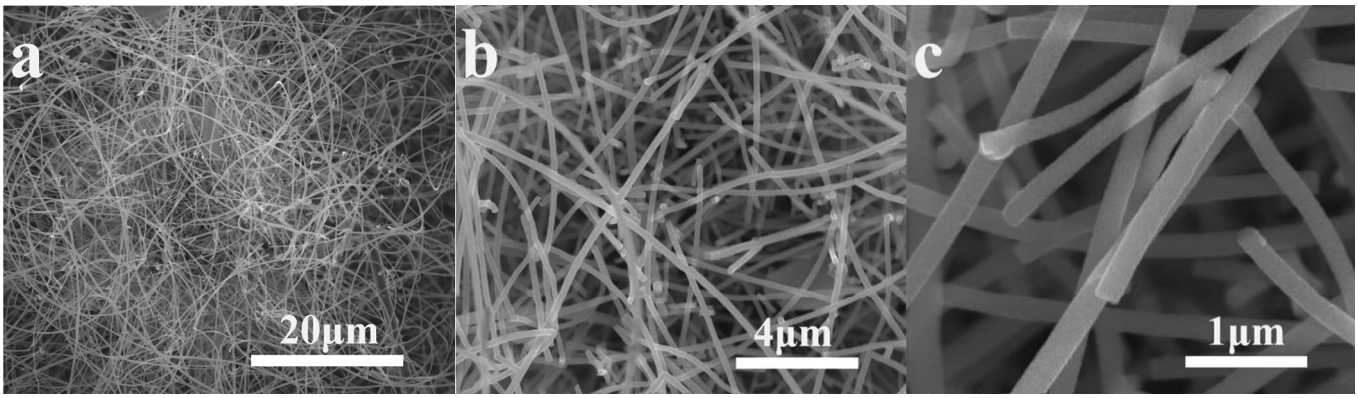

Fig. 1 SEM images of $La_xNd_{1-x}B_6$ nanowires synthesized at 1120ºC. (a) A general view of the nanowires. (b) A magnified SEM image of the nanowires. (c) Feature of nanowires surfaces and tips.

in a horizontal tubular furnace, which was equipped with a quartz tube of about 70mm in outer-diameter and 1170mm in length. Lanthanum and neodymium powders together with BCl_3 gas were used as the starting materials. La and Nd were weighed using an electronic scale on the basis of the calculation from atom ratio to mass percentage and thus guaranteeing their same atomic concentration. In brief, a totally 0.016g La and Nd powders were well-distributed on several Si wafers, while Si wafers were loaded in a quartz boat and was entirely put into the uniform temperature region of the long quartz tube subsequently. Before heating, quartz tube was evacuated and washed with a mixed gases (30% H_2+70% Ar, volume percent calculation). Then we designed a temperature control program to make a heat velocity of 15ºC per minute tardily to 1120ºC. The temperature was kept for 50min during which the BCl3 gas was introduced at a rate of 20 sccm. Finally, the temperature was allowed to descend gradually to room temperature. And then, representative samples were produced on the substrates. The final products which were gray in color, were immersed into hydrochloric acid solution for 2h and then transferred into double distilled water to wash several times to remove the H_3BO_3 and other unwanted byproducts. All procedures were conducted in constant pressure.

The samples were examined by FE-SEM, XRD, TEM, HRTEM, element mapping, EDS, and Raman Scattering. X-ray powder diffraction (XRD) analysis were carried out on a TD3500 X-ray diffractometer equipped with Cu Kα radiation (1.5419 Å), and the operation voltage and current were maintained at 30 kV and 20 mA, respectively. The surface morphology of the samples were observed by a Navo NanoSEM430 Field emission-Scanning electron microscope (FE-SEM). Transmission electron microscope (TEM) images were acquired on a JEM-2010HR TEM at an accelerating voltage of 200kV and a high-resolution transmission electron (HRTEM) Tecnai™ G^2 F30 at an accelerating voltage of 300kV. The chemical compositions were analyzed using energy dispersive spectrometer (EDS, Oxford instrument) attached to F30. The Raman Scattering spectra were recorded on a micro-Raman spectrometer (Renishaw inVia) at an excitation wavelength of 632.18nm.

The field emission performance of $La_xNd_{1-x}B_6$ nanowires was measured in a vacuum chamber at a pressure of ~10^{-7} Torr at room temperature. The process was conducted on a parallel-plate-electrode with stainless-steel probe (radius=0.2mm) as anode. The nanowires grown on Si substrate was used as cathode. The separation distance of anode from $La_xNd_{1-x}B_6$ nanowire's surface was fixed at 300μm. In the measuring circuit, emission current was directly recorded using Keithley 2400.

Results and discussion

Representative morphologies of the as-synthesized $La_xNd_{1-x}B_6$ nanowires, as revealed by FE-SEM, are illustrated in Fig. 1. The overview image was taken from the SEM in low-magnification mode (shown in Fig. 1a), which unambiguously shows that the prepared ultra-long large-scale $La_xNd_{1-x}B_6$ nanowires are flexibly and uniformly distributed on the substrates without any adherent impurities. While the image at high-resolution that manifests the surfaces and tips of $La_xNd_{1-x}B_6$ nanowires is presented in Fig. 1b, the wires diameters is 170-180nm and length is up to several hundred micrometres. One can see smooth surfaces and clean tips without any small particles formed from droplets in Fig. 1c. High aspect ratio of the nanowires manifests their possible excellent field emission property.

X-ray diffraction pattern is illustrated in Fig. 2a. The above curve represents $La_xNd_{1-x}B_6$ nanowires fabricated at 1120℃. And the standard diffraction patterns of LaB_6 and NdB_6 are demonstrated in the bottom. It can be seen that no impurities peaks were detected, which suggests the high purity of the synthesized products. As inset of Fig. 2a, the magnification of the strongest peak of $La_xNd_{1-x}B_6$ nanowires is right between the standard patterns peaks of LaB_6 and NdB_6 because of the different atom size of La and Nd. The X-ray diffraction pattern of $La_xNd_{1-x}B_6$ nanowires was successfully indexed with a cubic lattice using the program Dicvol, and the lattice parameters

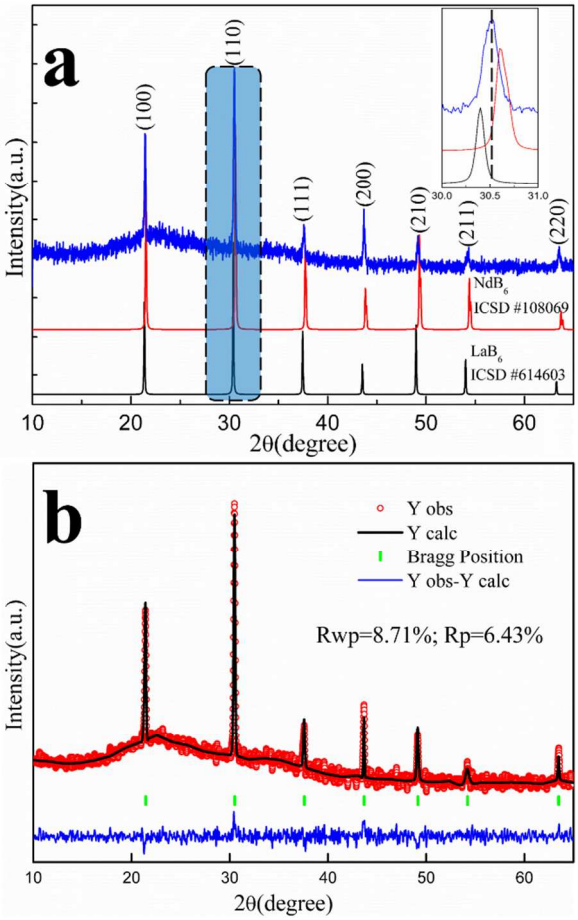

Fig. 2 (a) XRD pattern of $La_xNd_{1-x}B_6$ synthesized at 1120ºC. (b) *Rietveld* analysis of the sample.

Table 1 Structure parameters of standard LaB_6 and NdB_6, and $La_xNd_{1-x}B_6$ data is determined from *Rietveld* refinement.

Formula	Lattice constant (Å)	Unit cell volume (Å^3)	Reference
$La_xNd_{1-x}B_6$	4.142(5)	71.086(5)	This work
LaB_6	4.155	71.732	19
NdB_6	4.128	70.343	20

Table 2 The atomic sites and coordinates of $La_xNd_{1-x}B_6$ calculated from the *Rietveld* refinement.

Atoms	Wyckoff sites	a	b	c	Occupancy
La/Nd	1(a)	0	0	0	1
B	6(f)	0.450(10)	0.5	0.5	1

were further least-square refined by the program PIRUM. The space group of $La_xNd_{1-x}B_6$ compound was derived to be *Pm-3m* based on the reflection conditions. Table 1 illustrates the lattice constant and the unit cell volume of $La_xNd_{1-x}B_6$ and the data of LaB_6 and NdB_6 is also given for comparison. The lattice parameter of $La_xNd_{1-x}B_6$ is 4.142(5) Å, which is right between the standard lattice constant of LaB_6 (4.155 Å)[19] and NdB_6 (4.128 Å)[20] that complies well with *Vegard*'s law.[21] The number of chemical formula per unit cell of the $La_xNd_{1-x}B_6$ compounds is 1. Preliminary refinements of the cubic structure have been performed by *Rietveld* method[22] for $La_xNd_{1-x}B_6$ compound. The refinement results is shown in Fig.2b and the atomic parameters of $La_xNd_{1-x}B_6$ are given in Table 2. There are one rare-earth position (1(a)), one boron site (6(f)). Result of the Rietveld refinement of the crystal structure of $La_xNd_{1-x}B_6$ compound reveals that 1(a) position is occupied by 1 La(/Nd) randomly and 6(f) by 6B. The XRD results manifest the well-doped and uniform structure of the samples.

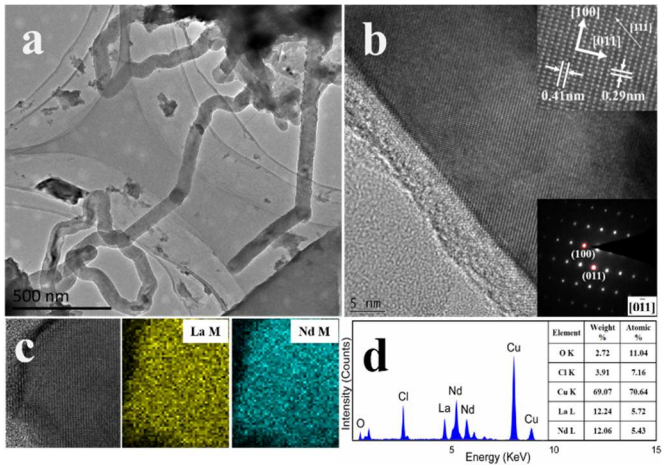

Fig. 3 TEM images of $La_xNd_{1-x}B_6$ samples synthesized at 1120ºC: (a) TEM image. (b) HRTEM image, top-right corner inset shows the magnification of a section of bulk area and the inset below is the corresponding SAED pattern. (c) HRTEM image and the corresponding elemental mapping of La and Nd. (d) EDS of the area shown in (a).

Further morphology study of $La_xNd_{1-x}B_6$ nanowires is presented in Fig. 3, with the TEM operated at 200kV for low-magnification and 300kV for high-magnification, respectively. Fig. 3a is a low-magnification TEM image where the dimensional feature is displayed. The smooth surfaces are reconfirmed apart from some bends and kinks that caused by the sample preparation. HRTEM (Fig. 3b) of $La_xNd_{1-x}B_6$ nanowires suggests the sample's highly crystalline nature that is devoid of any screw dislocations or stacking faults. The thin amorphous shells existed should be attributed to the deposition of boron species on the surfaces of rare earth metals and then prevent the localized vaporization of metals, thus at the same time producing amorphous boron surrounding the nanowires since this is the only feasible amorphous phase among the three elements.[12,23]According to the zoom-in HRTEM of the insets in the top-right corner, two groups of mutually perpendicular interference fringes can be seen clearly and the lattice d-spacings are calculated to be 0.41nm and 0.29nm that correspond perfectly to the (100) and (011) crystal faces of the XRD results. Another group of interference fringe with angles constituted with (100) and (011) lattice planes of both ~45° is also observed and the d-spacing is calculated to be ~0.24nm, which all manifest the [111] growth direction of these nanowires. The [111] orientation has been suggested to be a better alternative for field emitter gun filaments due to its better stability.[24] Selected area electron diffraction (SAED) was also applied to further illustrate the atom structure, as shown in the inset of Fig. 3b, the homogeneous image indicates the single crystal nature of the $La_xNd_{1-x}B_6$ nanowires, and the calculated lattice parameter agrees well with our XRD results. Additionally, the elemental mappings indicates the uniform distribution of La and Nd in the samples, suggesting the well-doped and uniform structure of $La_xNd_{1-x}B_6$ nanowires (Fig. 3c). Fig. 3d shows the EDS of the area in Fig. 3a, both La and Nd peaks are apparently presented in the spectrum. The weak

oxygen signal shown in the image may come from the little oxidization of La and Nd powder before putting into the tubular furnace. Strong copper peaks can be detected because of the Cu nets used as the TEM sample matrix during the performing process. The Cl peak observed is probably due to the decomposition and migration of the BCl_3 raw material. No B peak is observed in the EDS spectrum and this should attribute to the detection limit of EDS. Quantitative analysis was shown in the Table inset of Fig. 3d. The atomic percentages of La and Nd that manifest their actual concentration are 5.72% and 5.43%, respectively. And the ratio is calculated to be approximately 1 that matches the raw materials proportion as well as *Rietveld* refinement results where the occupancy ratio of La and Nd atoms at 1(a) site nearly equal to 1. Combined with XRD pattern (Fig. 2) as well as the HRTEM (Fig. 3(b)) and SAED (Fig. 3(b)-inset), these results serve as puissant evidences for the successful synthesis of uniform structured $La_xNd_{1-x}B_6$ nanowires and powerfully reconfirm the well-doped feature of $La_xNd_{1-x}B_6$.

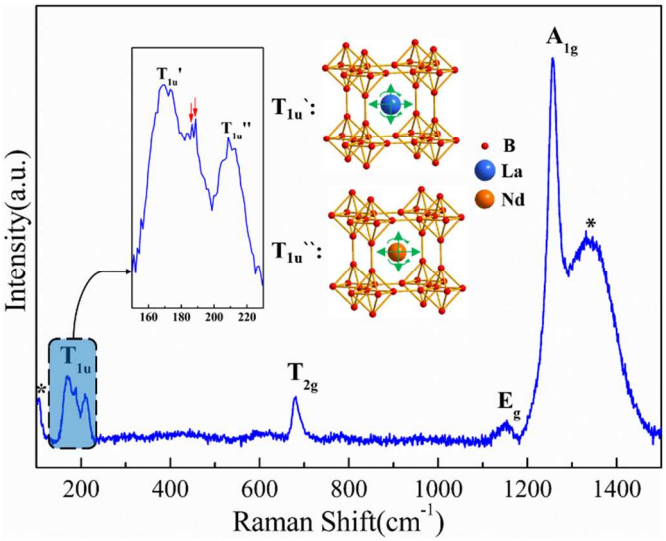

Fig. 4 Micro-Raman Scattering spectrum of $La_xNd_{1-x}B_6$ nanowires synthesized at 1120℃.

Micro-Raman spectrometer was conducted to depict the room temperature Raman Scattering property of $La_xNd_{1-x}B_6$ nanowires, as presented in Fig. 4. The sample was measured in the range of 100~1500 cm^{-1}. Owing to the cubic symmetry feature which determined by space group of *Pm-3m* of rare earth hexaborides, the lattice vibration modes can be summarized as follows according to the selected rule: $\Gamma=A_{1g}+E_g+T_{1g}+T_{2g}+2T_{1u}+T_{2u}$, while A_{1g}, E_g and T_{2g} can be attributed to the Raman-active phonons. Two T_{1u} modes are infrared-active, and T_{1g} and T_{2u} are optically inactive.[25-27] According to Fig. 4, A_{1g}, E_g and T_{2g} can be labelled easily at 1256 cm^{-1}, 1150 cm^{-1} and 681 cm^{-1}, respectively, conforming well to the previous reported data.[28] They can be attributed to the different vibration modes of boron octahedra in $La_xNd_{1-x}B_6$ structure. The three prominent peaks are additional confirmation for the formation of hexaborides. T_{1u} can be regarded as the vibration of rare-earth ions in octahedral B_6 cage.[25] According to the magnification of T_{1u} peak shown in the inset of Fig. 4 (black arrow directed), two peaks at 168 cm^{-1} and 208 cm^{-1} labelled as T_{1u}` and T_{1u}`` can be assigned to the vibration of La ions and Nd ions in octahedral B_6 cage on account of the dual-rare earth metal,[29-30] respectively. And the possible vibration modes are schematized in the crystal structure (inset in Fig. 4) that includes the rare-earth ions displacement.[25] The other two small peaks marked by red arrows in the inset of Fig. 4 can be assigned as the second-order Raman excitations of T_{1u}` phonon and T_{1u}`` phonon at Brillouin zone boundary, respectively.[25] The mode <200 cm^{-1} and a broad peak near 1400 cm^{-1}, denoted by asterisks, are commonly observed for trivalent and intermediate-valent crystals.[25-30] The relatively intense and sharp peaks shown in Fig. 4 prove that the nanowires are highly crystalline, which is consistent with the XRD and HRTEM results.

To date, there are many kinds of growth mechanisms proposed in vapor deposition system. Conventional vapor-liquid-solid (VLS) method is usually used in noble-metal or transition-metal catalyst-related systems, with nanosized catalysts observed embedded or attached to the tips of the synthesized samples.[31-33] Therefore, this traditional mechanism is ruled out in view of the smooth and flawless nanowires in SEM and TEM images. Nevertheless, the forming process can analogize to the typical VLS system in this catalyst-free system and it is rational to postulate that La-Nd alloy serve as reactants and catalysts simultaneously. Equilibrium phase diagram of La-Nd demonstrates the eutectic point of ~825 ºC at the La/Nd proportion of nearly 1,[34] which is much lower than the melting point of both La (920 ºC) and Nd (1024 ºC). As a result, at reaction temperature of 1120 ºC, La/Nd mixture can get a higher vapor pressure than a single component system and this is believed to be beneficial for the growth of nanowires. Although detailed information on the ternary phase diagram of La-Nd-B is not available,[35] small miscible La-Nd-B liquid alloy droplets

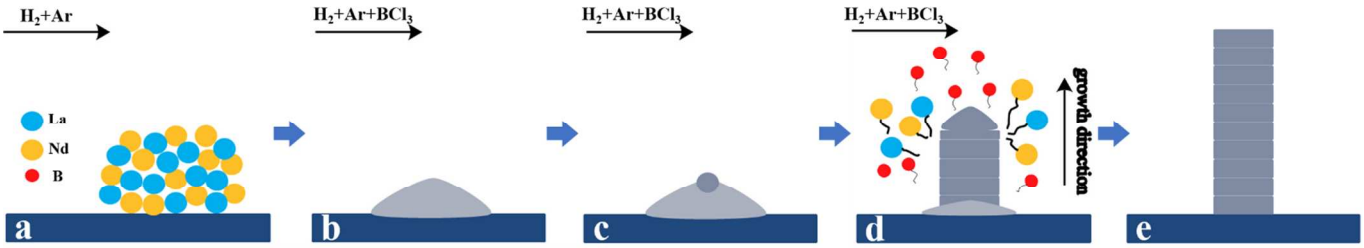

Fig. 5 Schematic model of nanowire growth. (a) La and Nd metal powders are uniformly distributed on silicon substrates. (b) As the temperature reaches the corresponding eutectic point of La-Nd alloy, the metals start to melt and large quantities of liquid droplets are formed. (c) B-containing molecules decomposed from inlet flow of BCl_3 start to be absorbed by the droplets on their surface to form nanoclusters serving as nuclei for nanowires growth in next episode. (d) Continuing augment of B, La and Nd vapor pressure makes them supersaturate to precipitate as $La_xNd_{1-x}B_6$ nanowires and keep growing. (e) Growth terminates when the source metals are exhausted.

Journal Name RSCPublishing

ARTICLE

may be formed and act as nucleation sites. The continuous supply of boron causes the liquid La-Nd-B droplets to become supersaturated until the raw materials exhausted, resulting in the precipitation of $La_xNd_{1-x}B_6$ nanowires. The growth procedure is described as follows, according to the model sketched in Fig. 5. The rare earth metals were originally introduced on silicon wafers under mild inlet gas stream of H_2/Ar (Fig. 5a). At elevated temperature, the metals are melted and La-Nd alloy droplets with size close to that of the initial solid raw metals particles start to form (as shown in Fig. 5b & c). Larger liquid droplets may develop naturally by agglomeration of several original small droplets. Meanwhile, B-containing molecules are continuously imported through the inlet gas flow and are supposed to be absorbed by the droplets on their surface, resulting in there being some nanoclusters, which subsequently serve as nuclei for nanowires growth. See Fig. 5d, the vapor pressure of La and Nd in the system keep increase to make the droplets become supersaturated, which supply the kinetics requirement for their precipitation as nanowires. As visualized in Fig. 5e, nanowires continue to grow as long as sufficient quantities of B-containing species and the source rare earth metal reactants are available. The growth finally terminates once the source metals are exhausted entirely. SEM images of samples at different reaction time (see Fig. S1, ESI) can better verify the growth procedure.

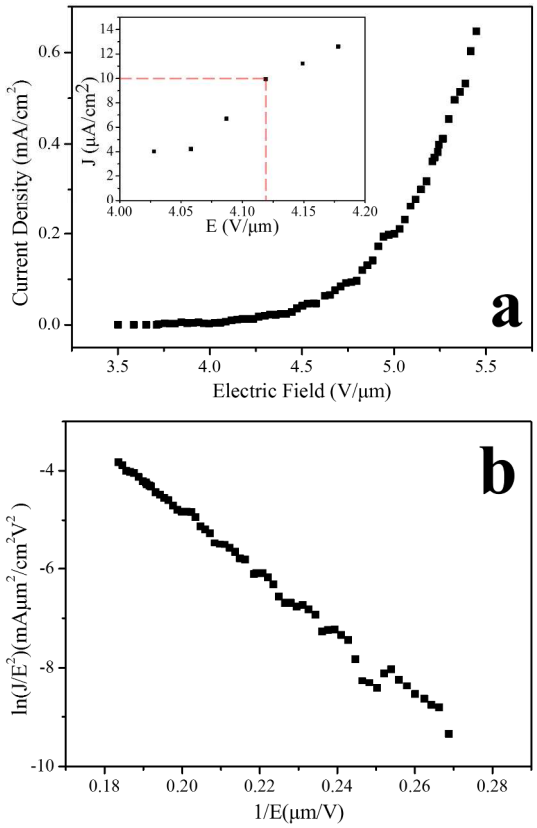

Fig. 6 Field emission performance of $La_xNd_{1-x}B_6$ nanowires emitter. (a) The exponential dependence of field emission current density *J vs* applied electric field strength *E*. Turn-on field of ~4.12V/μm is shown in inset. (b) Linear relationship of Fowler-Nordheim plot.

Table 3 Comparison of typical FE properties between $La_xNd_{1-x}B_6$ nanowires and others.

Materials	Synthesis method	Turn-on field [at 10μA/cm²]	Reference
B nanowires	Thermal-evaporation	5.1	36
Si nanowires	Thermal-evaporation	7.3	37
Mo nanowires	CVD	5	38
ZnO nanowires	CVD	5.6	39
SiC nanowires	Thermal-evaporation	10.1	40
WO_3 nanowires	Thermal-evaporation	4.8	41
LaB_6 nanorods	CVD	4.62	17
NdB_6 nanowires	CVD	5.55	16
$La_xNd_{1-x}B_6$ nanowires	CVD	4.12	This work

To investigate the performance of $La_xNd_{1-x}B_6$ nanowires as a field emitter for the first time, a preliminary examination of

FE properties was carried out in this work, as shown in Fig. 6. It can be seen that the emission current density J ascends exponentially with the increasing electric field E in Fig. 6a. The electron emission turn-on field (E_{to}), which is defined to be the macroscopic electric field required to generate a current density of 10μA/cm^2, is about 4.12V/μm according to inset in Fig. 6a. This data is lower than that of previously reported LaB_6 (E_{to}=4.62 V/μm)[17] and NdB_6 (E_{to}=5.55 V/μm)[16] by us and that may be attributed both to the factors of composition and morphological variation.[42] Such data also suggest $La_xNd_{1-x}B_6$ nanowires may rival those other inorganic nanostructures as a potential field emission cathode material (see Table 3). While the relative high E_{to} in comparison with carbon nanotubes might be mainly attributed to the random alignment of the nanowires as well as the poor conductivity of Si substrate etched by BCl_3 gas. The intrinsic values of E_{to} should probably be much lower than the value obtained this work. The existence of amorphous boron layer is positive for field emission performance according to the investigation of Zhang *et al.* in *Ref.* 12. However, the E_{to} of even crystalline boron nanowires is 5.1V/μm,[43] which is worse than that of $La_xNd_{1-x}B_6$ nanowires. This suggests that the field emission from the $La_xNd_{1-x}B_6$ nanowires should mainly result from the crystalline part of the nanowires rather than the amorphous boron layer. The field emission current-voltage characteristic of $La_xNd_{1-x}B_6$ nanowires is further analysed on the basis of the typical F-N model,[8] from which the relationship between current density (J) and applied electric field (E) can be described as follows:

$$J = A(\frac{\beta^2 E^2}{\Phi})\exp(\frac{-B\Phi^{3/2}}{\beta E}) \qquad (1)$$

where A= 1.54×10^{-10}AV^{-2}eV, B=6.83×10^7 Vcm^{-1} eV$^{-3/2}$, β is the field enhancement factor and Φ is the work function of the emitting material. Fig. 6b indicates the linear dependence of $\ln(J/E^2)$ *vs* $1/E$ (the F-N plot), confirming the F-N tunnelling emission mechanism.

Attempts were also made to understand the morphological influence of reaction duration, reaction temperature and proportion of La, Nd powders. The detailed information are as follows. Fig. S1 (see the ESI) represent the typical morphologies of products fabricated with different time duration in reaction temperature of 1120ºC. According to Fig. S1a, b, c & d, the morphological evolution is apparently presented that from melted particles, short-straight nanorods to curly nanowires, to high aspect ratio nanowires. The evolution process can also reflect the growth procedure to some extent.

Reaction temperature is another significant parameter that strongly affects the final morphology of the corresponding sample. As illustrated in Fig. S2 (ESI), the morphologies shown in Fig. S2a & b are samples fabricated at 1115ºC and 1125ºC. Typically, at a low reaction temperature of 1115ºC, short-straight nanorods with diameters of ~200-400nm and length ranging from 800nm to several micrometres were formed (Fig. S2a, ESI). After upgrading the synthesis temperature by 10 degree centigrade, as shown in Fig. S2b (ESI), long-curled wire-like nanostructured $La_xNd_{1-x}B_6$ were fabricated. The curled wires distribute sparsely on cubic-like bulks and stretched to several tens micrometres with diameters varying from 200nm-220nm. The quite different sights manifest their morphologies sensitivity to temperature during growth.

Proportions of reactants La, Nd powders is of importance in determining the shapes of synthesized samples. The eutectic point is about 825 ºC with the La/Nd proportion of nearly 1 if the phase relation of La-Nd binary system was concerned.[34] Here, X-ray diffraction patterns illustrated in the inset of Fig. S3a & b (ESI) suggest that single phase $La_xNd_{1-x}B_6$ can also fabricated with different La/Nd powders atomic proportion. However, as shown in Fig. S3 (given in the ESI), submicron-sized $La_xNd_{1-x}B_6$ cubes were fabricated when proportions of La/Nd reactants powders departs from the eutectic composition. The quite different shapes may be caused by the diverse growth mechanism in the formation process if the eutectic composition was deviated. And the submicron-cubes were probably developed through Ostwald ripening process,[28] during which larger particles would grow continually at the cost of smaller ones to reduce the total surface free energy according to the well-known Gibbs-Thomson law.[44-45]

Conclusions

In summary, $La_xNd_{1-x}B_6$ nanowires were synthesized by a catalyst-free CVD method and further characterized by XRD, FE-SEM, HRTEM, SAED, element mapping, EDS and Raman Scattering and all of the results affirmed their uniform and well-doped nature. Several parameters correlated in the experiments, i.e. temperature, reaction time and proportion of La, Nd powders, were surveyed trying to understand the controllable synthesis possibility and to better elucidate the growth mechanism. The experimental results prove that well-distributed uniform $La_xNd_{1-x}B_6$ nanowires were hard to be formed in our present conditions except samples synthesized at 1120ºC, 50 mins reaction time and La/Nd reactants proportion of 1. A dominantly VLS-like mechanism with self-catalytic growth mechanism was postulated to depict the formation process of $La_xNd_{1-x}B_6$ nanowires, on the basis of some experiment results in the present work. Preliminary field emission test had been done on $La_xNd_{1-x}B_6$ nanowires and the relatively low turn-on field of ~4.12V/μm demonstrate their potentials as new candidates for application in optoelectronic devices such as flat panel displays and nanoelectronics building blocks.

Acknowledgements

This work was funded by NSFC Grant (No. 51372089, 51172077, 51373205) supported through NSFC Committee of China, and the Foundation of (No. 2014ZB0014, No. 2013ZM0111) supported through the Fundamental Research Funds for the Central Universities.

Notes and references

[a] *State Key Laboratory of Luminescent Materials and Devices, South China University of Technology, Guangzhou, 510641, PR China*

[b] *Instrumental Analysis and Research Centre, Sun Yat-Sen University, Guangzhou, 510275, PR China*

*Corresponding author. E-mail: puscj@mail.sysu.edu.cn; zhaoym@scut.edu.cn

† Footnotes should appear here. These might include comments relevant to but not central to the matter under discussion, limited experimental and spectral data, and crystallographic data.

Electronic Supplementary Information (ESI) available: [details of any supplementary information available should be included here]. See DOI: 10.1039/b000000x/

1 R. Gomer, *Field Emission and Field Ionization*, Harvard University Press, Cambridge, Mass., 1961.

2 T. Y. Zhai, L. Li, Y. Ma, M. Y. Liao, X. Wang, X. S. Fang, J. N. Yao, Y. Bando and D. Golberg, *Chem. Soc. Rev.*, 2011, **40**, 2986.
3 X. S. Fang, Y. Bando, U. K. Gautam, C. H. Ye and D. Golberg, *J. Mater. Chem.*, 2008, **18**, 509.
4 Y. Yang, H. Yang, G. D. Wei, L. Wang, M. H. Shang, Z. B. Yang, B. Tang and W. Y. Yang, *J. Mater. Chem.* C, 2014, **2**, 4515.
5 I. J. Teng, H. L. Hsu, S. R. Jian, C. T. Kuo and J. Y. Juang, *Nanoscale*, 2012, **4**, 7362.
6 B. B. Wang, K. Ostrikov, T. van der Laan, K. Zheng, J. J. Wang, Y. P. Yan and X. J. Quan, *J. Mater. Chem. C*, 2013, **1**, 7703.
7 J. M. Lafferty, *J. Appl. Phys.*, 1951, **22**, 299.
8 R. H. Fowler and L. W. Nordheim, *Proc. R. Soc. London A*, 1928, **119**, 173.
9 H. Zhang, Q. Zhang, J. Tang and L.-C. Qin, *J. Am. Chem. Soc*., 2005, **127**, 2862.
10 H. Zhang, Q. Zhang, G. Zhao, J. Tang, O. Zhou and L.-C. Qin, *J. Am. Chem. Soc*., 2005, **127**, 13120.
11 H. Zhang, Q. Zhang, J. Tang and L.-C. Qin, *J. Am. Chem. Soc*., 2005, **127**, 8002.
12 H .Zhang, J. Tang, Q. Zhang, G. Zhao, G. Yang, J. Zhang, O. Zhou and L.-C. Qin, *Adv. Mater.*, 2006, **18**, 87.
13 J. R. Brewer, N. Deo, Y. M. Wang and C. L. Cheung, *Chem. Mater*., 2007, **19**, 6379.
14 G. Wang, J. R. Brewer, J. Y. Chan, D. R. Diercks and C. L. Cheung, *J. Phys. Chem. C*, 2009, **113**, 10446.
15 J. R. Brewer, R. M. Jacobberger, D. R. Diercks and C. L. Cheung, *Chem. Mater*., 2011, **23**, 2606.
16 Q. H. Fan, Q. Y. Zhang, Y. M. Zhao and Q. W. Ding, *J. Rare Earths*, 2013, **31**, 145.
17 J. Q. Xu, Y. M. Zhao and Q. Y. Zhang, *J. Appl. Phys*., 2008, **104**, 124306.
18 H. Nagata, K. Harada and R. Shimizu, *J. Appl. Phys*., 1990, **68**, 3614.
19 A. Berrada, J.-P. Mercurio, J. Etourneau and P. Hagenmuller, *MRS Bull*., 1976, **11**, 947.
20 C. M. McCarthy and C. W. Tompson, *J. Phys. Chem. Solids*, 1980, **41**, 1319.
21 R. N. Musin and X. Q. Wang, *Phys. Rev. B*, 2005, **71**, 155318.
22 V. F.-Nicolin and R. Cerny, *J. Appl. Crystallogr*., 2002, **35**, 734.
23 T. T. Xu, J. G. Zheng, A. W. Nicholls, S. Stankovich, R. D. Piner and R. S. Ruoff, *Nano Lett*., 2004, **4**, 2051
24 T. Takigawa, I. Sasaki, T. Meguro, K. Motoyama, *J. Appl. Phys*., 1982, **53**, 5891.
25 N. Ogita, S. Nagai, N. Okamoto, M. Udagawa, F. Iga, M. Sera, J. Akimitsu and S. Kunii, *Phys. Rev. B*, 2003, **68**, 224305.
26 N. Ogita, S. Nagai, N. Okamoto, F. Iga, S. Kunii, J. Akimitsu and M. Udagawa, *Physica B*, 2003, **328**, 131.
27 N. Ogita, S. Nagai, M. Udagawa, F. Iga, M. Sera, T. Oguchi, J. Akimitsu and S. Kunii, *Physica B*, 2005, **359–361**, 941.
28 R. K. Selvan, I. Genish, I. Perelshtein, J. M. C. Moreno and A. Gedanken, *J. Phys. Chem. C*, 2008, **112**, 1795.
29 J. Q. Xu, G. H. Hou, H. Q. Li, T. Y. Zhai, B. P. Dong, H. L. Yan, Y. R. Wang, B. H. Yu, Y. Bando and D. Golberg, *NPG Asia Materials*, 2013, **5**, e53.
30 J. Q. Xu, G. H. Hou, T. Mori, H. Q. Li, Y. R. Wang, Y. Y. Chang, Y. S. Luo, Y. B. Yu, Y. Ma, T. Y. Zhai, *Adv. Funct. Mater*., 2013, **23**, 5038.
31 R. S. Wagner and W. C. Ellis, *Appl. Phys. Lett*., 1964, **4**, 89.
32 Y. N. Xia, P. D. Yang, Y. G. Sun, Y. Y. Wu, B. Mayer, B. Gates, Y. D. Yin, F. Kim and Y. Q. Yan, *Adv. Mater*., 2003, **15**, 353.
33 S.S. Brenner and G. W. Sears, *Acta Metall*., 1956, **3**, 268.
34 K. A. Gschneidner jr and F. W. Calderwood, *Bull. Alloy Phase Diagrams*, 1982, **2**, 452.
35 P. Villars, A. Prince, H. Okamoto, *Handbook of Ternary Alloy Phase Diagrams*, ASM International: Materials Park, OH, 1995.
36 J. F. Tian, Z. C. Xu, C. M. Shen, F. Liu, N. S. Xu and H. J. Gao, *Nanoscale*, 2010, **2**, 1375.
37 X. S. Fang, Y. Bando, C. H. Ye, G. Z. Shen, U. K. Gautam, C. C. Tang and D. Golberg, *Chem. Commun.*, 2007, 4093.
38 J. Zhou, S. Z. Deng, L. Gong, Y. Ding, J. Chen, J. X. Huang, J. Chen, N. S. Xu and Z. L. Wang, *J. Phys. Chem. B*, 2006, **110**, 10296.
39 Z. Q. Wang, J. F. Gong, Y. Su, Y. W. Jiang and S. G. Yang, *Cryst. Growth Des.*, 2010, **10**, 2455.
40 G. Z. Shen, Y. Bando, C. H. Ye, B. D. Liu and D. Golberg, *Nanotechnology*, 2006, **17**, 3468.
41 Y. Baek and K. Yong, *J. Phys. Chem. C*, 2007, **111**, 1213.
42 Menaka, R. Patra, S. Ghosh and A. K. Ganguli, *J. Solid State Chem.*, 2012, **194**, 173
43 F. Liu, J. F. Tian, L. H. Bao, T. Z. Yang, C. M. Shen, X. Y. Lai, Z. M. Xiao, W. G. Xie, S. Z. Deng, J. Chen, J. C. She, N. S. Xu and H. J. Gao, *Adv. Mater.*, 2008, **20**, 2609.
44 J. Zeng, H. Wang, Y. C. Zhang, M. K. Zhu, H. Yan, *J. Phys. Chem. C*, 2007, **111**, 11879.
45 J. W. Mullin, *Crystallization*, 3rd ed, Butterworth-Heinemann: Oxford, U.K., 1997.

Graphical Abstract

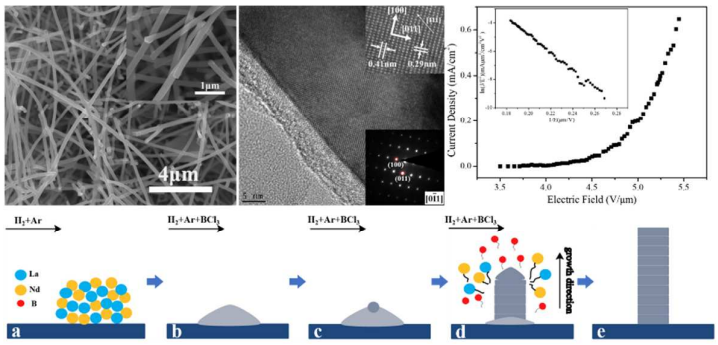

Structurally uniform and well-doped single crystalline $La_xNd_{1-x}B_6$ nanowires were fabricated and evaluated as a field emission cathode material for the first time.